



A Comparative Study on the Prediction of Bow Flare Slamming load using CFD and Prescript Formula for the Container Ship[†]

Dae-Won Seo^{1*}, Gi-Young Jeon¹, and Kang-Hyun Song¹

¹*Korean Register of Shipping, Busan, Korea*

(Manuscript Received October 18 2018; Revised November 15, 2018; Accepted December 20, 2018)

Abstract

A ship repeatedly face free surface under rough sea conditions owing to relative motion with wave encounter. The impact pressure is transferred to the hull structure and causes structural damage. In this study, the bow flare slamming load of a container ship is estimated using computations fluid dynamics (CFD) and prescript formula according to various classifications. It is found that the bow flare slamming load calculated by the formulas of the common structural rule and ABS tends to be similar to the CFD results.

Keywords: Bow flare slamming; Container Ship; Finite Volume Method; Finite Element Method; Strain Rate Effects

1. Introduction

A ship repeatedly face free surface under rough sea conditions owing to relative motion with wave encounter. In the process of entering into water, the ship structure is temporarily subjected to the impact pressure. The impact pressures are categorized into bow flare slamming, bottom slamming, stern slamming, and green water loading depending on the position where the impact occurs, and various studies have been carried out using calculations and model experiments. In general, bow flare slamming occurs often in large container ships with a large flare angle, stern slamming frequently occurs on LNGCs since they have a relatively wide stern, and bottom slamming occurs in tankers because they have blunt stems. Repeatedly applied impact pressure causes structural damage and affects the stability of the vessel.

It is important to estimate the impact load of the slamming phenomenon. Von Karman (1929) and Wagner (1932) tried to find an asymptotic solution to the slamming pressure on a 2D circular cylinder and wedge shapes long ago. Since then, studies based on the potential flow have been conducted to predict the slamming impact pressure by Dobrovol'skaya (1969), Zhao and Faltinsen (1998). However, there is a difficulty in simulating the breaking wave using the potential code when the free surface hits the hull structure. Since then, many studies have been conducted to estimate the slamming impact pressure including the breaking wave by model experiments and computational fluid dynamics (CFD). Wang et al. (1996) measured the slamming pressure through a model experiment on the drop test of a wedge and tried to investigate the relationship between slamming pressure and dead rise angle. Various studies have been conducted recently, and Hong et al. (2008) examined a model experiment of the drop test on the 2D wedge section and the 2D

[†] This paper was presented at the 8th International conference on The 8th Hydroelasticity In Marine Technology (HYEL 2018), Seoul, Korea, September, 2018.

* Corresponding author. E-mail address: dwseo@krs.co.kr

Copyright © KSOE 2018.

Table 1. Principal parameters of the container ship

	Ship	Model
Scale ratio	1	31.599
Lpp [m]	230	7.2786
B [m]	32.2	1.019
T [m]	10.8	0.3418
Δ [m ³]	52030	1.649
LCG	111.6	3.532
VCG [m], from keel	14.322	0.453
Kxx/B	0.4	
Kyy/Lpp, Kzz/Lpp	0.25	

bow section in particular. Hong et al. (2014) also conducted a model experiment to measure bow flare slamming on container ships in regular and irregular waves. Wang and Guedes Soares (2012, 2013) confirmed that numerical results on slamming pressure agreed well with those of drop tests of the wedge through a model experiment. Lee and Lew (2015) and Kim et al. (2008) conducted the calculation using CFD on an LNG C and container ship. However, it is still difficult to accurately estimate the impact pressure through numerical simulations, because the slamming pressure occurs suddenly and disappears in a matter of seconds. In particular, it is necessary to keep the delta time of CFD sufficiently small, and the total calculation time increases significantly.

A significant motion of the vessel and intense free water surface have to be measured accurately to estimate the slamming load reliably. Although studies, which predicted the slamming pressure, were conducted often under irregular wave conditions in the real ship scale [Chen and Chen (2014), Wang and Soares (2016)], this is deemed impractical to be applied to the design phase considering the calculation time for simulation. Therefore, simplifications of irregular waves to regular waves under head sea conditions and simplified interpretations using incident waves have become common [ABS, 2002].

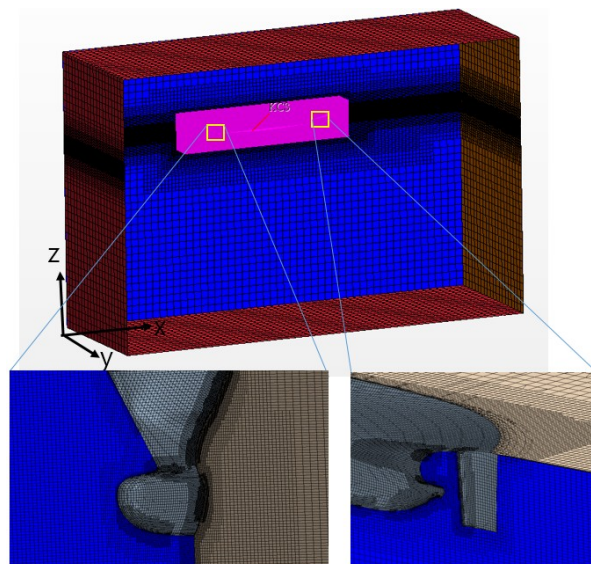


Fig. 1 Overset mesh system on the container ship

The subject vessel of this study is a KCS container ship with various experimental data. Recently, experimental results of additional resistance in regular waves were published at a CFD workshop held in Japan in 2015, and they were widely used for the verification of numerical simulations. Unfortunately, experiments on measuring the slamming pressure have not been performed yet, and the results of this numerical study are expected to be the basis of comparable data in terms of prediction of slamming load.

The slamming pressure from the numerical simulation was directly compared with the formula proposed by various classification society rules. These results are expected to be the data base for the revision of slamming load formulas in the future.

2. Numerical Setup and Calculation Conditions

The target vessel is a container with a length of 230 m. Numerical simulations were performed on a 1/31.599 scale ratio. The longitudinal center of gravity (LCG) is 111.6 m based on AP and the vertical center (VCG) of gravity is 14.322 m from the keel (Table 1).

A grid generation and a numerical simulation were carried out using STAR-CCM+ Version 11.06 in the commercial code. The trimmed mesh method has the advantage because the mesh size can be set either relatively small for complex flow ranges or large in cases of simple flow ranges through the configuration control of the mesh density in accordance with each flow characteristic used.

The calculation of the spatial gradient of the physical amount in a polyhedral grid made according to a trimmed mesh uses the least square method for second order accuracy. Moreover, to simulate the boundary layer flow on the surface of the ship relatively accurately, we used the prism layer technique to grid layers with 4.4 million grids from the hull surface by the half-width model ship, as shown in Fig. 1.

The generation of the incident wave is an important factor in estimating the slamming pressure accurately. Abdussamie et al. (2014a, 2014b) studied the grid dependency on the wave generation and found that more than 30 grids for the wave height and 80 grids for the wave length were needed to generate the waves well numerically. Therefore, 50 grids for the wave height and around 100 grids for the wave length were used in the numerical simulations.

The numerical calculation used the Stokes fifth order considering the wave height and period. The Euler overlay method (EOM) was also applied to simulate waves accurately without numerical damping. The wave that passes through the ship is naturally damped from the rear in the analysis domain to minimize the impact of reflection from the rear boundary.

A symmetric condition was applied to the free surface position ($Z = 0$) and the side of the calculation domain, while the wall condition was applied to the surface of the ship. The volume of fluid method was used to reflect the free surface.

A dynamic fluid body interaction (DFBI) scheme was applied to simulate the motion of the ship by the wave. Except for the heave and pitch motion, all other motions were fixed. An overset grid system was also used to simulate accurately a large ship motion by waves. An overset mesh allows complex motion and moving parts to be easily set up and simulated. An overset mesh typically containing a body of interest, such as boat, is superimposed on a background mesh containing the surrounding geometry, and data are interpolated between the two. Many researchers use the overset mesh system for slamming phenomena or ship motion due to waves [Ock (2014)].

An equivalent design wave method was used to select the target wave height, and the target wave period was considered as relative motion (Fig. 2). Six degrees of freedom motion of the KCS container ship used KR3D, the motion analysis program based on the potential theory, owned by the KRS. Based on the calculated motion of the ship, the response amplitude operators (RAOs) were derived for relative motion of the FP and incident wave. The wave that had the greatest impact on the slamming at the bow flare was limited as the incident wave (180°), and the target wavelength was set by the wavelength with the greatest relative motion. To determine the wave height of the incident wave, North Atlantic Standard Wave Data (IACS Rec. No. 34) and PM Spectrum were used to calculate the long term with a probability level of 10^{-8} and then divide that by the maximum value of the relative motion.

Table 2 Test conditions for numerical simulation

Vs	5 knots
Wave height	20.7 m
Wave period	12.57 s
Wave heading	180°

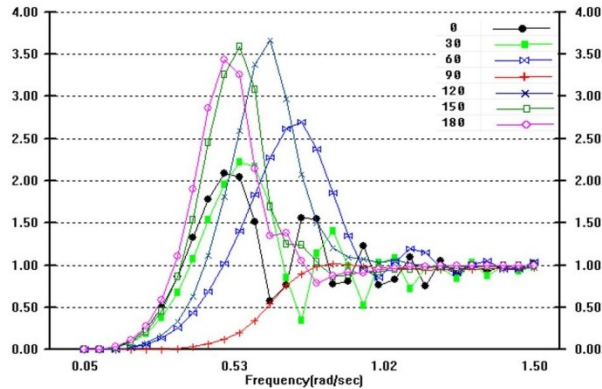


Fig. 2 RAOs of the relative motion at the bow

The numerical calculation was carried out under the condition of a wave period of 12.57 s and a wave height of 20.7 m, as shown in Table 2.

3. Validation of the Numerical Setup

Impact pressure prediction through the CFD analysis is generally known to be most influenced by the time step (Δt) and the grid resolution (Peric and Zorn (2005)). The time step is known to be the most dominant factor affecting the impact pressure prediction through the CFD analysis in general. In this study, prior to estimating the slamming pressure on the 3D vessel, the validity of the numerical calculation was investigated in order to improve the accuracy of the impact pressure estimation on the free fall of a wedge-shaped body with reliable experimental results.

3.1 Target Object

A wedge-shaped body was selected to examine the validity of the numerical setup. The length and breadth of the wedge-shaped body are 800 mm and 600 mm, respectively. The wedge angle is 30°, as shown in Fig. 3. For the measuring point and further detailed information, refer to Kim et al. (2014).

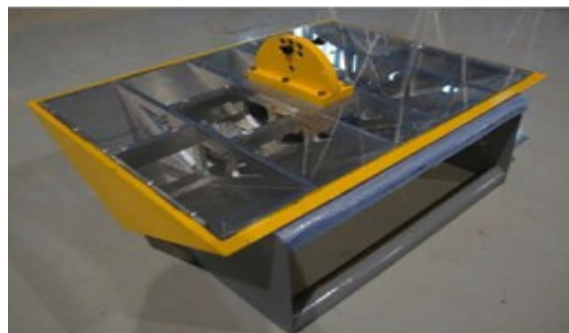


Fig. 3 Experiment on the 2D wedge (Kim et al., 2014)

Table 3 Test conditions of the various grid systems

	$\Delta x, \Delta y$ [m]	B/Y_{cell}	dt [s]
Coarse	0.01	60	5×10^{-5}
Medium	0.005	120	
Fine	0.0025	240	

3.2 Influence of the Grid Size

A numerical simulation was carried out to investigate the effect of the grid size on the prediction of the impact pressure, as shown in Fig. 4. The grid size is defined as B/Y_{cell} . B/Y_{cell} of the coarse mesh, medium mesh, and fine mesh are 60, 120, and 240, respectively, as shown in Table 3. B is the breadth of the wedge-shaped body, and Y_{cell} is the minimum grid size in the direction of the breadth. The time step of the numerical simulation is fixed at 5×10^{-5} (20 kHz), which is the same value as the measured velocity of the sensor used in the model test.

The influence of the grid size on the estimation of the impact pressure is shown in Fig. 5. As shown in the figure, the results of the numerical simulation show that the maximum pressure and characteristics are similar to the experimental results. In all cases of the numerical calculations, pressure oscillations were generated as compared to the experiment, but this was because the experimental results were processed through a filter. Above the medium grid size, the peak pressure value was found to match that of the experimental values within a range of approximately 3%. However, the point of occurrence of the peak pressure and the absolute value in the case of the coarse mesh were found to be significantly different from those of the experimental results. Based on the results of this analysis, the grid size was constructed to be greater than 120 of B/Y_{cell} when calculating the slamming impact pressure of a 3D vessel in this study.

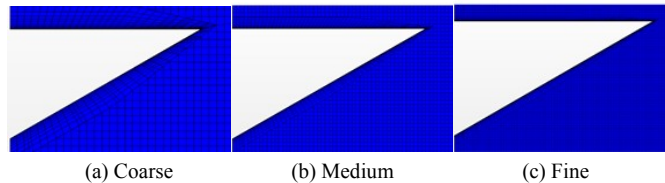


Fig. 4 Grid system for various numbers of cells

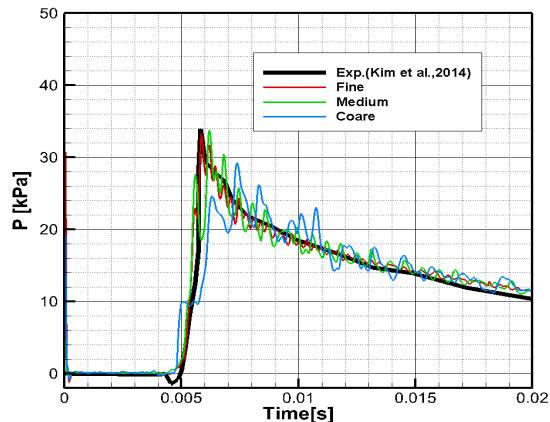


Fig. 5 Comparison of the pressure history on various grid systems

Table 4 Test conditions for various time steps (dt)

dt [s]	Courant No.	$\Delta x, \Delta y$ [m]
1×10^{-5}	0.006	0.005
5×10^{-5}	0.03	
1×10^{-4}	0.06	
1×10^{-3}	0.6	

3.3 Influence of the Time Step

It is known that the estimation of the impact pressure acting on the hull for an extremely short period of time is greatly affected by the time step conditions in numerical calculations. Therefore, numerical simulations for four cases were additionally carried out to examine the influence of the time step on the size and aspect of the impact pressure. From the study on the free fall experiment of a wedge-shaped body by Kim et al. (2014), the Courant number is 0.006 when the time step is the smallest with approximately 1×10^{-5} s. As such, we performed the calculation under four conditions of the Courant number = 0.006, which divided the rise time by 100, Courant number = 0.03, which divided the time step by 20, Courant number = 0.06 which divided the time step by 10, and Courant number = 0.6, which was the time step, as shown in Table 4.

Fig. 6 shows the estimated calculated results of the impact pressure measured over time in the experiment and from the numerical simulation. As seen in the figure, the predicted maximum pressure value was considerably lower than the experimental results when the Courant number = 0.06. However, the impact pressure pattern tends to be similar to the results of the model test in all cases except for this case. In particular, when the Courant number was lower than 0.03, the maximum impact pressure from the numerical results was in good agreement with the experimental results quantitatively. When the Courant number was 0.06, the maximum peak pressure was about 30k Pa and 10% lower compared to that of the model test, but the rise time and the duration of pressure from the numerical results were shown to be almost the same as the experimental ones. From the perspective of the efficiency of the numerical calculation, it was decided that the results of the numerical calculation were also meaningful even when the Courant number was 0.06. As we determined that the case when the Courant number = 0.06 was also significant for the efficiency of the numerical analysis, we used 0.06 for the Courant number to calculate the slamming of the ship.

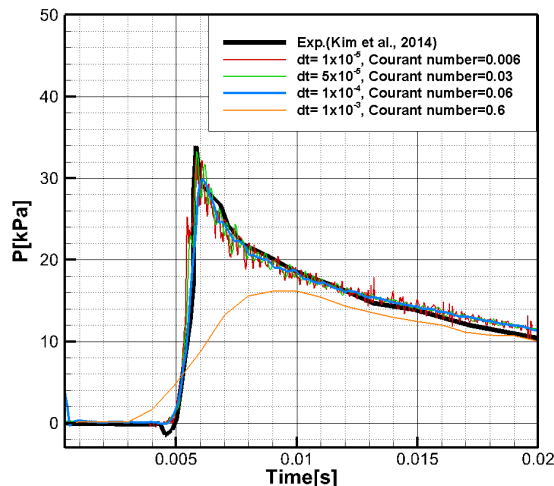


Fig. 6 Comparison of the pressure history on various delta times

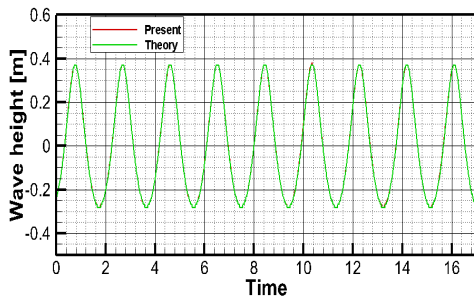


Fig. 7 Comparison of the wave height generated by the CFD and theory methods ($V_s = 5$ knots, $H = 20.7$ m, and $T = 12.57$ s)

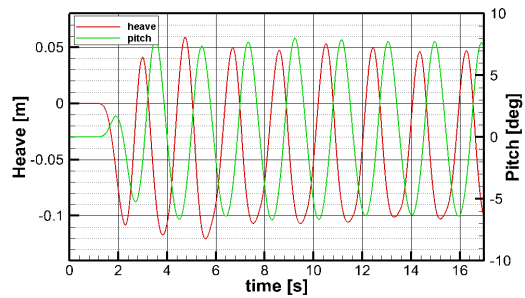


Fig. 8 Time history of the heave and pitch motion on the KCS ship ($V_s = 5$ knots, $H = 20.7$ m and $T = 12.57$ s)

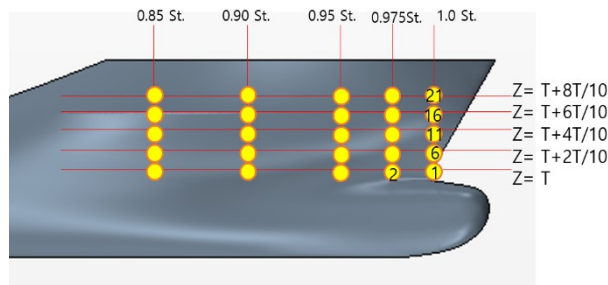


Fig. 9 Pressure measuring points of the numerical simulation

4. Results of the Numerical Calculations

4.1 Incident Wave and Ship Motion

In ships operating under rough sea conditions, the impact pressure is applied on the hull because of the relative motion with incident waves. Hence, it is necessary to implement accurate incident waves for numerical simulations of slamming phenomena. Fig. 7 compares the wave elevation measured by the CFD and that obtained by a theoretical method at a $0.5 L$ distance away from the FP, in the direction of the entrance of the vessel towards the stern. As shown in this figure, it can be confirmed that the incident wave to be generated is properly implemented in the numerical simulation. This is because the waveform compensation using the EOM method and the generated grid system has the sufficient grid density per wave length and height.

In this study, motions of the vessel caused by 180° incident waves were performed in heave and pitch motion as free condition in head sea, as shown in Fig. 8. For the stability of the numerical solution, the motion of the ship was virtually forced for about 2 s. The pitch angle and heave motion of the ship change from -6.3° to 7.6° and from -0.103 m to 0.046 m with regular waves, respectively.

4.2 Bow Pressure

As shown in Fig. 9, it was divided into five sections from FP to 0.85 St. and into five sections based on the draft to measure the impact pressure. The bow impact pressure was measured at a total of 25 measuring points.

Fig. 10 shows the slamming pressure acting on the 25 points as described above. A high impact pressure of 10 kPa was mainly observed near the free surface, as shown in Figs. 10 (a–c). In the upper region, the impact pressure was not high, as shown in Figs. 10(d) and 10(f). The highest peak pressure was measured at FP 12 point around 14.75 s.

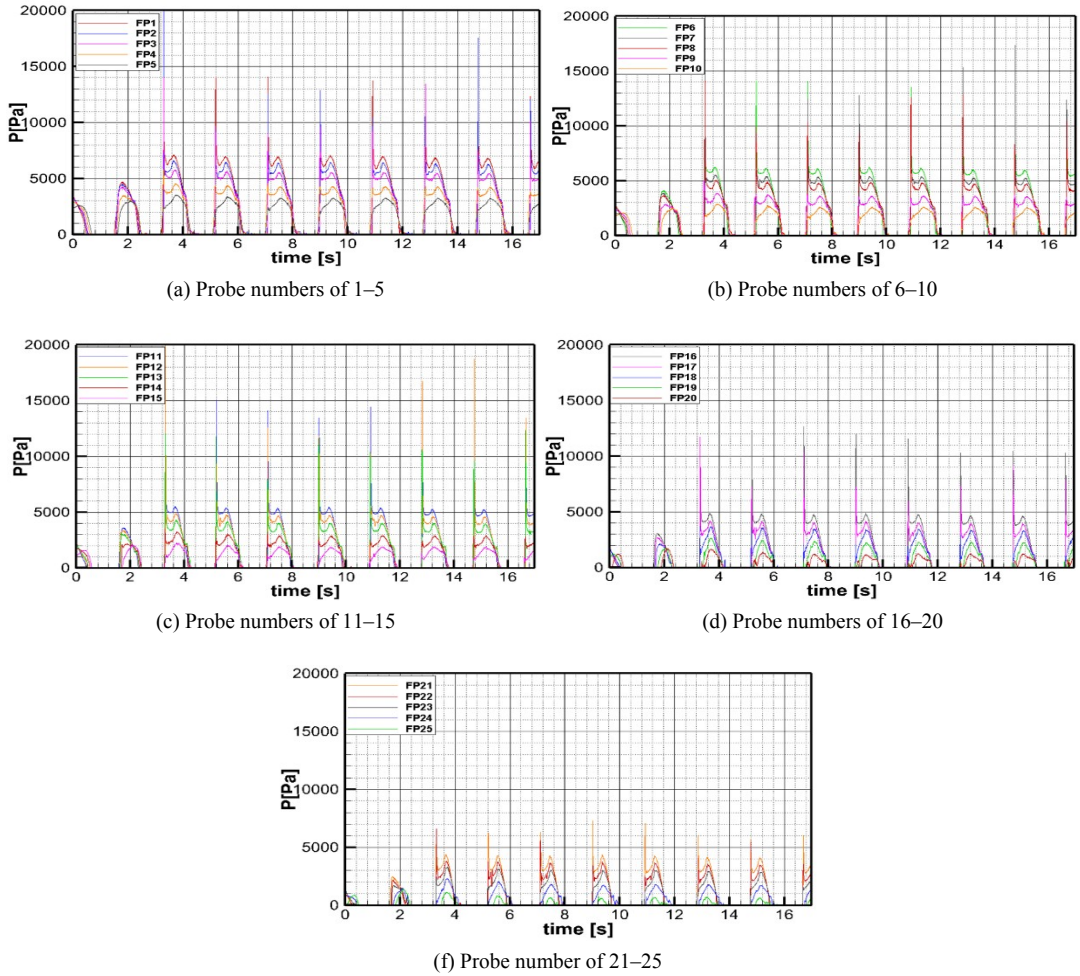


Fig. 10 Pressure time history at specific points

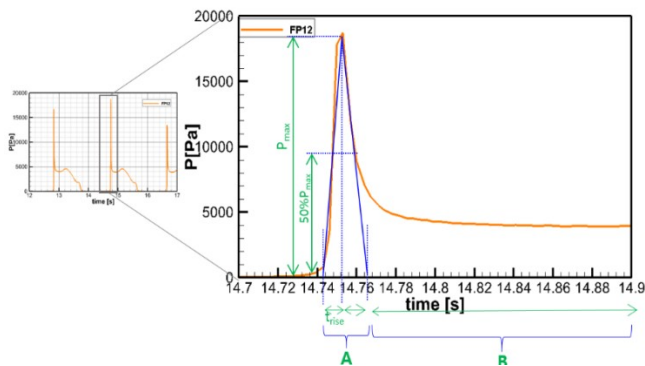


Fig. 11 Pressure time history at FP12

Fig. 11 shows the time history of the pressure at the FP12 point where the maximum peak pressure is observed. As shown in the figure, the impact pressure temporarily increases and then disappears in region A.

Table 5 Categorization of the slamming formulas in the classification

Class	Rule	Bow flare	Bottom	Stern
IACS	Bulk, Tanker	O (only bow)	O	-
ABS	Container	O	O	-
BV	Container	O	O	O
DNV-GL	Ships	O	O	O
LR	Ships	O	O	O
NK	Steel ship	O	O	-

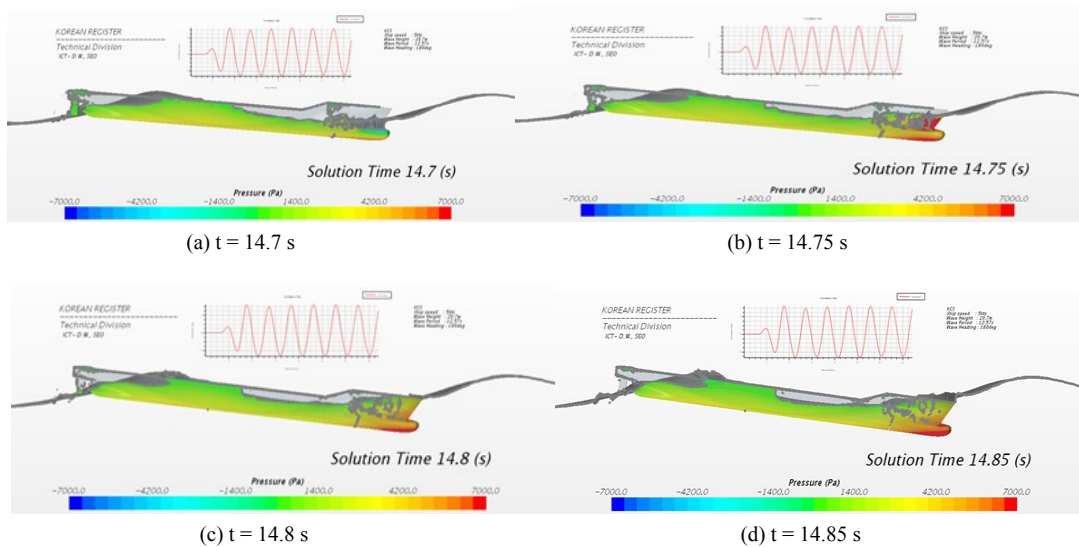


Fig. 12 Pressure distributions and free surface

In region B, the static pressure is constantly maintained after the impact pressure has passed. The total duration time of the impact pressure is expressed as the sum of the rise time (t_{rise}) and drop time (t_{drop}), which is about 0.023 s (0.13 s in the full scale). The duration time of the B region due to the static pressure is approximately 0.93 s (5.23 s in the full scale). The maximum peak pressure acting on the FP12 point is approximately 18.75 kPa and is approximately 592 kPa in the full scale.

5. Classification Rules

5.1 Slamming Pressure Formula for Each Classification

As shown in Table 5, each classification has proposed a formula of the slamming pressure acting on the hull. All formulas of the classification adequately take into account the water-entry impact pressure due to vertical relative motion and the breaking wave impact pressure due to the velocity component in the forward direction. In this study, the results of the predicated slamming pressure by IACS, ABS, BV, DNV, LR, and NK, which applied the rules for various classifications, were compared and reviewed.

The common structural rule (CSR) in the international classification society defines the bow slamming pressure equation, as shown in Eq (1). The CSR is a common rule developed to be applied to cargo ships and tankers, but it was also applied to container ships, the objects of this study, for relative comparison and

analysis.

$$P_{FB} = 1.025 f_{FB} C_{FB} V_{im}^2 \sin \gamma_{wl} \quad (1)$$

where f_{FB} is the coefficient of the impact pressure distribution in the longitudinal direction and V_{im} represents the impact velocity, which is a function of LBP, Vs, and waterline angle. γ_{wl} means the flare angle (IACS, 2014).

The rule of the ABS classification provides an empirical formula of the bow slamming pressure due to the wave, and also provides the bow flare slamming pressure, as shown in Eq. (2) (ABS, 2016).

$$\begin{aligned} P_{ij} &= P_{oij} \text{ or } P_{bij} \\ P_{oij} &= k_1 (9M_{Ri} - h_{ij}^2)^{1/2} \\ P_{bij} &= k_2 k_3 \{ C_2 + K_{ij} M_{Vi} [1 + E_{ni}] \} \end{aligned} \quad (2)$$

where M_{Vi} is a function of LBP, Vs, and Cb; K_{ij} is a function of the waterline angle and flare angle. Unlike other classification rules, the breadth at the considered point is reflected, and this uniquely requires the breadth of the bow shape.

The rule of the BV classification provides an empirical formula of the bow flare slamming pressure, as shown in Eq. (3).

$$P_{Fl} = C_s C_L C_Z (0.22 + 0.15 \tan \alpha) \times (0.4V \sin \beta + \sqrt{L})^2 \quad (3)$$

The feature of this formula is that the characteristics of a structural part (C_s) are considered when calculating the bow flare slamming pressure, but the length, direction, and location have no relation to the pressure (BV, 2017). The coefficient (C_z) that reflects the upward position is applied to consider relative motion, but the vessels of this study have all constant values.

Equation 4 is the empirical formula of the bow flare slamming pressure in the DNV-GL classification and is similar to the rule of BV.

$$P_{sl} = C(2.2 + C_f) \times (0.4V \sin \beta + 0.6\sqrt{L})^2 \quad (4)$$

where C_f is the factor that reflects the roll and pitch motion of the ship, and the design load of the rule should be referred to DNV-GL (2016).

In the LR classification, the empirical formula of the bow flare slamming pressure is provided, as shown in Eq. (5). The formula is a function of the coefficient considering the bow shape and the relative vertical velocity (LR, 2017)

$$IP_{bf} = 0.5 (K_{bf} V_{bf}^2 + K_{rv} H_{rv} V_{rv}^2) \quad (5)$$

The empirical formula of the bow slamming pressure in the NK classification is defined, as shown in Eq. (6) (NK, 2016).

$$P = \frac{1}{2} \rho C_e K_p \left(\frac{v_n}{\cos \beta_0} \right)^2 \quad (6)$$

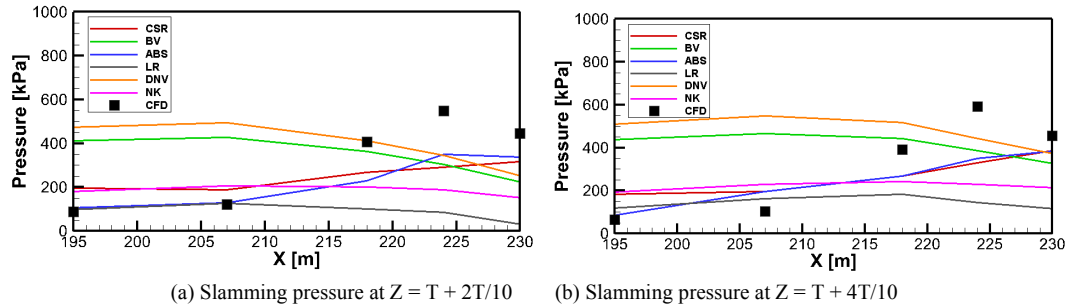


Fig. 13 Comparison of the slamming pressure calculated using various formulas of the classifications

5.1 Comparison of the Bow Flare Slamming Pressures

The empirical formulas in various classifications provide the quasi-static pressures without impact pressure. Hence, it is unreasonable to compare the maximum impact pressure calculated in CFD with the quasi-static pressure calculated using the prescript formula. Though it is decided insignificant to make the direct comparison of the absolute value of the quasi-static pressure proposed by a classification with the maximum value of the dynamic pressure derived from numerical calculations, the maximum value of the dynamic pressure from the numerical calculations and the slamming pressure are shown in Fig. 13, to observe qualitative characteristics in investigating the tendency of the slamming pressure on the hull.

The numerical results show that the bow flare slamming pressure increases from 0.9 St. ($X = 207$ m) to FP ($X = 230$ m) and the maximum impact pressure is generated at 0.975 St. ($X = 225$ m). The tendency of the pressure to increase towards the forward direction was similar to the results of ABS and CSR. Except for other results of the ABS and CSR rules, it is found that the slamming pressure is rather decreased in the direction of the FP, which demonstrated a relatively different tendency from the results of the numerical calculations.

6. Conclusion

Prior to a numerical simulation on a container ship, a numerical calculation was conducted to examine the validities of the numerical code on a reliable model test. A numerical simulation was performed to predict the bow slamming pressure on the container ship under extreme wave conditions ($H = 20.47$ m and $T = 12.57$ s), and these results were compared to the empirical formulas of different classifications.

1) In order to obtain relatively quantitative numerical calculation results, the grid density (B/Y_{cell}) should be 120 or greater, and the Courant number should be 0.06 or smaller.

2) The position that generated the maximum impact pressure is around 0.95 St., and the maximum impact pressure is measured momentarily at FP12 near the bow region. The maximum peak pressure acting on the FP12 point is approximately 18.75 kPa and is approximately 592 kPa in the full scale. The duration time of the impact pressure is 0.13 sin the full scale. The static pressure continues to act as the bow descends below the free surface by pitch motion.

3) Though it is unreasonable to directly compare the absolute value of the quasi-static pressure proposed by a classification with the maximum value of the dynamic pressure derived from numerical calculations, from the point of view of qualitative tendency, the results of the ABS and CSR classifications showed that the impact pressure was significantly increased in the FP direction similar to the results of the numerical simulation.

Acknowledgements

This work was supported by the Industrial Strategic Technology Development Program (10073164) funded by the Ministry of Trade, Industry & Energy.

References

- Abdussamie, N., Amin, W., Ojeda, R., Thomas, G., and Drobyshevski, Y., 2014(a). Vertical Wave-in-Deck Loading and Pressure Distribution on Fixed Horizontal Decks of Offshore Platforms. *The 24th International Offshore and Polar Engineering*, Busan, South Korea.
- Abdussamie, N., Ojeda, R., Amin, W., Thomas, G., and Drobyshevski, Y., 2014(b). Prediction of Wave-in-Deck Loads on Offshore Structures Using CFD. *The 19th Australasian Fluid Mechanics Conference*, Melbourne, Australia, 8–11.
- ABS, 2016. *Rules for building and classing Steel Vessels*, Part 5C, Section 3.
- ABS, 2002. *A Direct Calculation Approach for Designing a ship-shaped FPSO's Bow Against Wave Slamming Load*, Technical Report.
- BV, 2017. *Structure Rules for Container ships*, Chapter 4, Section 5.
- Chen, C.R. and Chen, H.C., 2014. CFD simulation of Extreme Slamming on a Containership in Random Waves. *The 24th International Ocean and Polar Engineering Conference*, Korea.
- DNV-GL, 2016. *Rule for Classification of Ships- Hull structural design Ships with length 100 meters and above*, Part.3 Chapter 1, Section 7.
- Dobrovolskaya, Z.N., 1969. On some problems of similarity flow of fluids with a free surface. *Journal of Fluid Mechanics*. 36, 805–829.
- Hong, S.Y., Kyoung, J.H., Kim, Y.S., Song, K.-H., Kim, S., Malenica, S., Lindergren, M., Rathje, H., and Ge, C., 2008. Validation of wave loads on a large container ship in oblique waves. *The 6th Osaka Colloquium on Seakeeping and stability of ships*, Osaka, 109–117.
- Hong, S.Y., Kim, K.H., Kim, B.W., and Kim, Y.S., 2014. Experimental Study on the Bow-Flare Slamming of a 10,000 TEU Containership. *Proc. the 24th Int. Ocean and Polar Engineering Conference*, Busan, Korea.
- IACS, 2014. *Common Structural Rules for Bulk Carriers and Oil Tankers*, Part 1, Chapter 4, Section 5.
- Kim, K., Shin, Y.S., and Wang, W., 2008. A Stern Slamming Analysis Using Three-Dimensional CFD Simulation. *The 27th International Conference on Offshore Mechanics and Arctic Engineering*, Estoril Portugal.
- Kim, K.H., Lee, D.Y., Hong, S.Y., Kim, B.W., Kim, Y.S. and Nam, B.W., 2014. Experimental study on the water impact load on symmetric and asymmetric wedges, *The 24th international Ocean and Polar Engineering Conference*, 15-20 June, Busan, Korea, 2014, ISOPE-I-14-336.
- Lee, S. and Lew, J., 2015. Numerical Computations of Impact Forces Acting on Breakwater Plate of Bow Deck of Container Carrier. *Journal of the Society of Naval Architects of Korea*, 52(3), 198–205.
- LR, 2017. *Rules and Regulations for the classification of Naval Ships*, Part 4, Chapter 2, Section 4.
- Muzaferija, S., Peric M.P., Sames, P., and Schellin, T., 1998. A Two Fluid Navier-Stokes Solver to Simulate Water Entry, *The 22nd Symposium on Naval Hydrodynamics*, Washington D.C., USA, 638–651.
- NK, 2016. *Rules for the Survey and Construction of Steel Ships*, Part C, Chapter 6.
- Ock, Y.B., 2014. *Numerical Simulations of Added Resistance around Ships in Regular Head Waves using Overset Grids*, Master's thesis, Department of Naval Architecture and Ocean Engineering, Pusan National University.
- Peric, M. and Zorn, T.: Simulation of sloshing loads on moving tanks, 2005. *24th International Conference on Offshore Mechanics and Arctic Engineering*, 12-17 June, Halkidiki, Greece, 2005, OMAE2005-67581.
- Von Kármán, T., 1929. *The impact on sea plane floats during landing*. *National Advisory Committee for Aeronautics*. Technical Note No 321, 309–313.
- Wagner, H., 1932. Über Stossund Gleitvergänge an der Oberfläche von Flüssigkeiten. *Z. Angew. Mathematik und Mechanik*. 12, 193–215.
- Wang, S. and Guedes Soares, C., 2012. Analysis of the water impact of symmetric wedges with a multi-material eulerian formulation. *International Journal of Maritime Engineering*, 154 (A4), 191–206.
- Wang, S. and Guedes Soares, C., 2013. Slam induced loads on bow-flared sections with various roll angles.

Ocean Engineering, 67, 45–57.

Wang S. and Soares, C.G., 2016. Stern slamming of chemical tanker in irregular head waves, *Ocean Engineering*, 122, 322–332.

Wang, R., Faltinsen, O.M., and Aarsnes, J.V., 1996. Water entry of arbitrary two-dimensional sections with and without flow separation, *The 21st Symposium on Naval Hydrodynamics*, 408–423.

Zhao, R. and Faltisen, O., 1998. Water Entry of Arbitrary Axisymmetric Bodies With and Without Flow Separation. *The 22nd Symposium on Naval Hydrodynamics*, Washington D.C., USA, 652–664.